
# Graphene nanospikes exert bactericidal effect through mechanical damage and oxidative stress

Carbon 218 (2024) 118740

Contents lists available at ScienceDirect

Carbon

journal homepage: www.elsevier.com/locate/carbon

# "Graphene nanospikes exert bactericidal effect through mechanical damage and oxidative stress"

Yanyan Chen [a], Santosh Pandit [a,*], Shadi Rahimi [a], Ivan Mijakovic [a,b,**]

[a] Systems and Synthetic Biology Division, Department of Life Sciences, Chalmers University of Technology, SE-412 96, Gothenburg, Sweden
[b] The Novo Nordisk Foundation, Center for Biosustainability, Technical University of Denmark, DK-2800, Kongens Lyngby, Denmark

ARTICLE INFO

*Keywords:*
Graphene nanospikes
Antibacterial surface
Biomimetic nanostructures
Genetically encoded ROS biosensors
Quantification of oxidative stress

ABSTRACT

Microbial contamination of biomedical surfaces is an important clinical challenge, driving the development of new antibacterial materials. Nanoprotrusions on the wing surface of some insects have intrinsic antibacterial and antifouling properties, which inspires fabrication of biomimetic nanopatterns on medical devices. Herein, we report a broad-spectrum bactericidal surface consisting of graphene nanospikes synthesized by plasma-enhanced chemical vapor deposition. Similar coatings have been reported before, but the killing mechanism and main parameters for efficiency of such coatings have not been clarified. We investigated the correlation of anti-biofilm efficiency of graphene nanospikes to their major physicochemical parameters. While height and thickness of nanospikes did not directly correlate with bactericidal effects, edge/defect density showed linear correlation with lethality for both Gram-negative and Gram-positive bacteria. We further demonstrated that the killing mechanism is synergistic, depending on physical rupture of bacterial membranes as well as considerable oxidative damage to the cells. Of note, for the first time, we quantify the level of oxidative stress induced by graphene nanospikes in two bacterial species using genetically encoded biosensors. Our work provides a fundamental understanding of the impact of various parameters of graphene nanostructures on the bactericidal efficiency, enabling rational design of graphene-based bactericidal surfaces.

## 1. Introduction

Infectious diseases have become the second leading cause of death worldwide [1]. Various surface functionalization strategies have been adapted to prevent the attachment, proliferation, and biofilm formation of infectious microorganisms [2,3]. Considering that leaching surfaces (releasing toxic chemical agents to surrounding area) have drawbacks such as ecological impact and exhaustion of loaded antibacterial chemicals, nonleaching surfaces which directly kill bacterial cells on contact are desirable for practical application [4].

Recently, the bactericidal nature of insect wings, gecko skin, and some plants has aroused much interest [5]. For instance, surface of cicada wings, covering by densely and regularly packed nanopillars with approximately 200 nm in height and 60 nm in diameter, shows selective toxicity against Gram-negative bacteria [6,7]. Similarly, nanopatterns have also been observed on dragonfly wing surfaces, along with a better killing efficiency against both Gram-positive and Gram-negative bacteria [8]. The enhanced biocidal activity has been attributed to randomness in size, shape, and distribution of nanoclusters on the surface of dragonfly wings. Mechanistic studies indicate that those nanoarrays, regardless of their chemical compositions and functionalities, cause physical stretch and rupture of bacterial membranes, leading to cell death without triggering any resistance [9,10]. Notably, mammalian cells with their much bigger sizes experience neglectable membrane stress upon contacting such surfaces [11,12]. Inspired by nature, artificial antibacterial nanostructures have been fabricated using metallic biomaterials [13], black silicon [9,14], carbon nanotubes (CNTs) [15], and polymers [12,16] to mimic those natural nanopatterns and to replicate their bactericidal property. With fine tuning of topographical parameters of nanostructures, biomimetic surfaces even surpass their natural counterparts in combating bacterial infections [17].

Graphene is an attractive 2D nanomaterial for biomedical applications owing to its outstanding properties, such as conductivity, mechanical stiffness, thermal stability, and biocompatibility [18]. A

* Corresponding author.
** Corresponding author. Systems and Synthetic Biology Division, Department of Life Sciences, Chalmers University of Technology, SE-412 96, Gothenburg, Sweden.
*E-mail addresses:* pandit@chalmers.se (S. Pandit), ivan.mijakovic@chalmers.se (I. Mijakovic).

https://doi.org/10.1016/j.carbon.2023.118740
Received 11 September 2023; Received in revised form 11 December 2023; Accepted 13 December 2023
Available online 19 December 2023

broad-spectrum antibacterial activity of graphene materials (GMs) has been demonstrated [19]. Mechanistic investigations claim that sharp edges of graphene are crucial for their toxicity [20,21]. On one hand, they act as "nano-knives" to physically damage cell membrane by extracting lipid molecules or punching pores on membrane. On the other hand, defects on the edge of graphene could oxidize cell membrane or intracellular components through production of reactive oxygen species (ROS) or direct electron transfer. This leads to oxidative stress in living cells and eventually cell death. Both the mechanical disruption and ROS stress caused by GMs are not prone to induce bacterial resistance, which makes GMs promising for fighting resistant pathogens [22]. Several examples of GM-based antibacterial surfaces maximizing edge/defect effects have been reported to date. Among those, Akhavan et al. reported that graphene oxide (GO) nanowalls deposited on stainless steel substrates via electrophoretic deposition had nearly perpendicular edges, causing the efflux of RNA of bacteria and cell death [23]. Ivanova et al. observed that the rough surface of exfoliated graphene film had better antibacterial behavior compared with its smooth surface, owing to more exposed edges [24]. Elimelech and coworkers enhanced the antibacterial activity of GO by aligning GO flakes vertically in 2-hydroxyethyl methacrylate (HEMA) polymer film using magnetic field [25]. Nevertheless, graphene-based antibacterial surfaces prepared by the above methods mainly involved multi-step and complex chemical procedures but ended up with relatively poor control over topographic characteristics of GMs. In this sense, plasma-enhanced chemical vapor deposition (PECVD), which is commonly used for mass production for graphene with good purity and high quality, provides a feasible, scalable, and low-cost technique for fabricating bactericidal graphene nanostructures with well-defined geometry [26]. Recently, vertical graphene nanostructures have been synthesized on various substrates by PECVD [27], some of which reported bactericidal effects [28–30]. The relation between specific physicochemical parameters of vertical graphene nanostructures and their bacterial toxicity is unclear. The toxicity mechanisms of graphene surfaces are yet to be understood [31]. Especially the controversy over oxidative stress triggered by graphene needs to be settled. In the available literature, small-molecule fluorescent probes were generally employed to detect ROS, as a proxy of oxidative stress. However, intrinsic limitations of those probes, such as the uneven uptake by living cells, limited selectivity, problems of quantification, photobleaching etc., make these results questionable [32]. For more reliable measurement of redox stress in living cells, genetically encoded biosensors have been developed [33–35]. However, such biosensors have not yet been used to investigate the contribution of redox stress to the antibacterial action of GM surfaces.

The aim of this work is to produce graphene nanospikes on silicon substrate and to investigate the relation between antibacterial activity and physicochemical parameters of graphene nanoflakes. We used PECVD method for a single-step growth of vertical graphene nanoarrays *in-situ*. The morphology of graphene arrays was characterized by scanning electron microscopy (SEM), transmission electron microscopy (TEM), and atomic force microscopy (AFM). Next, we assessed the surface parameters of graphene nanospikes, including height, thickness, and edge/defect density. The respective contributions of these parameters to antibacterial efficiency were determined as well. Finally, we investigated the underlying biocidal mechanism of graphene nanospikes. We observed morphology of bacteria after exposing to graphene surfaces under SEM. Genetically encoded biosensors were also employed to measure the dynamic concentration of major thiol-redox buffer in living bacterial cells, specifically, glutathione (GSH) in *E. coli* cells and bacillithiol (BSH) in *S. aureus* cells, providing a quantitative assay of oxidative damage triggered by graphene nanospikes.

## 2. Methods

### 2.1. Synthesis of graphene nanospikes

Graphene nanospikes were synthesized by plasma enhanced chemical vapor deposition (PECVD) on silicon wafer coated with 300 nm $SiO_2$ layer according to the previous report [28]. Briefly, the substrate (1 × 1 $cm^2$) was placed into a quartz chamber, heated up to 775 °C within 2 min under Ar (1000 sccm) and $H_2$ (30 sccm), and annealed for 1 min to clean the surface. Then, the growth of graphene was initiated by introducing a 75 W DC glow discharge plasma and a carbon source ethylene ($C_2H_2$, 15sccm). To produce graphene nanospikes with different surface nanofeatures, we controlled the growth time to be 10, 15, 20, 25, and 30 min, respectively. After growth, the chamber was quickly cooled down to room temperature under Ar and $H_2$ flow. The as-produced graphene nanospikes were directly used for further characterization and biological experiment without additional process.

### 2.2. Characterization of graphene surface

The morphology of graphene nanospikes was analyzed by SEM (JEOL JSM-6301F) under the acceleration voltage of 12 kV. And AFM (NT-MDT NTEGRA) was employed to measure the parameters of graphene nanospikes, including height, thickness, and aspect ratio. TEM was carried out using a FEI Tecnai T20 transmission electron microscope under the acceleration voltage of 200 kV. To prepare a TEM specimen, a copper grid was placed on graphene surface, pressed, and scratched for the manual transformation of the sample to TEM grid [36]. Raman spectra were measured using a WITec alpha300 R Raman Microscope equipped with a 532 nm laser, for the identification of atomic structure of graphene nanospikes and for the quantification of edge/defect density. The intensity of laser was set to 64 μW. The integration time was 1 s, and the accumulation time was 10. The surface wettability of graphene samples was evaluated by measuring the water contact angle in air using an optical goniometer (OneAttension, Biolin Scienfic). The needle diameter was 0.718 mm, and images were taken within 1–2 s of the droplet (approximately 5 μL in size) being dispensed on the sample. Graphene samples of three different batches were analyzed for reproducible data for each experiment.

### 2.3. Antibacterial activity of graphene nanospikes

*E. coli* (UTI89) and *S. aureus* (CCUG10778) were purchased from Gothenburg University Culture Collection (CCUG) and used for evaluation of anti-biofilm efficiency of graphene surfaces. The culture medium for the two bacterial species was Luria-Bertani (LB) broth and tryptic soy broth (TSB), respectively. Bacteria were grown in liquid medium at 37 °C overnight. Then an inoculum containing 2–5 × $10^6$ colony forming unit (CFU)/mL bacteria was made by diluting the overnight bacterial culture in fresh medium. 80 μL of the inoculum was transferred on the surface of each sample. To a control group, bacterial inoculum was put on the top of silicon substrate with 300 nm $SiO_2$ coating. After 24 h incubation in a 37 °C incubator, biofilms were formed on the substrates and were ready for analysis. Note that, to avoid evaporation of bacterial droplet on the substrate, 8 graphene samples were placed in the middle part of a 24-well plate, while the other 16 wells at the edges of the plate were filled with sterilized water.

A live/dead staining assay was carried out to analyze cell viability, as reported in previous works [15,25]. 24 h-old biofilms grown on the surface of each sample were firstly detached from the substrate to 5 mL saline solution (0.89 % NaCl) by sonication using a probe sonicator (250/450 Digital Sonifier, Branson) at 10 W for 30 s, following by three times washing and resuspended in 50 μL saline solution. Then, 6 μM SYTO 9 and 30 μM propidium iodide (LIVE/DEAD BacLight bacterial viability kit, Invitrogen) were added to the bacterial suspension to stain live and dead cells, respectively. After 20 min staining, cells were

pipetted to a microscope slide and images were taken using a fluorescent microscope (Axio Imager 2, Carl Zeiss). The fluorescence intensity of two channels were analyzed using Image J software and the percentage of dead cells were then calculated. For each sample, fluorescent images were taken for five random locations. Three independent biological replicates were assessed for each sample.

The biofilm killing efficiency of graphene nanospikes was evaluated using a colony counting assay. *E. coli* and *S. aureus* cells were cultured on the graphene coated and noncoated surfaces for 24 h, as described before for the live/dead staining assay. After removing bacteria adhered to the surfaces through sonication, the dissociated bacteria solution was diluted serially in saline solution to 1000-fold and then spread uniformly on LB agar and TSB agar for *E. coli* and *S. aureus*, respectively. The experiments were conducted in triplicate, and the mean values are reported. And the killing percentage was obtained by normalizing the CFU of each surface corresponding to that of silicon surface (control surface).

### 2.4. Mechanical rupture of bacterial membranes by graphene nanospikes

SEM (JEOL JSM-6301F) was used to visualize the morphological change of bacterial membranes after exposure to graphene nanospikes. Graphene nanospikes at a growth time of 20 min were exposed to bacteria (both *E. coli* and *S. aureus*) for 24 h, as described before. The biofilms were directly observed on the substrate without detaching from the surfaces. Briefly, biofilms were rinsed twice with saline solution, fixed by 3 % glutaraldehyde at room temperature for 2 h, and dehydrated by graded series of ethanol (30 %, 40 %, 50 %, 60 %, 70 %, 80 %, and 90 %) for 15 min each and by absolute ethanol for 20 min. The dehydrated samples were dried overnight at room temperature and sputter coated with 5 nm of gold layer before taking SEM images. SEM was performed with an acceleration voltage of 10 kV for all samples.

### 2.5. Oxidative stress detection and quantification

For direct detection of ROS in bacteria, a fluorescent ROS probe, CellRox deep red was purchased from Life Technology. Cells were cultured on graphene surface of a growth time of 20 min for 24 h before staining with CellRox deep red. To a control sample, bacteria were grown on silicon substrate for 24 h. And a positive control sample was obtained by further treating 24 hold biofilms with 100 mM $H_2O_2$ for 40 min. After 24 h incubation, biofilms on each substrate were detached by probe sonication, washed with 0.89 % NaCl solution and collected by centrifuge (5000 rmp, 5 min) before use. Then, the as-collected cells were stained with 5 μM ROS probe for 20 min according to the manufacturer's protocol, following by a counter stain with DAPI (5 μM, 20 min). After staining, three as-prepared samples were transferred to a microscope slide and observed under fluorescent microscope (Axio Imager 2, Carl Zeiss).

To quantify oxidative damage induced by graphene nanospikes, the real-time glutathione redox potential in Gram-negative bacteria and the bacillithiol redox potential in Gram-positive bacterial was monitored by genetically encoded biosensors, respectively. Specifically, pQE-60 Grx1-roGFP2-His plasmid, which was a gift from Tobias Dick (Addgene plasmid # 64,799; http://n2t.net/addgene:64,799; RRID: Addgene_64,799), was expressed in Gram-negative *E. coli* DH5alpha stain. And a Gram-positive *S. aureus* COL strain containing pRB437-XylR-Brx-roGFP2 plasmid was constructed and given by Haike Antelmann [34]. *E. coli* cells were cultivated in LB medium containing 100 μg/mL ampicillin (AMP). And *S. aureus* cells were grown in LB medium containing 1 % xylose and 10 μg/mL chloramphenicol (*Cm*). For the measurement of oxidative stress, a single colony of two bacterial strains was inoculated in 5 mL culture medium and grown at 37 °C in a shaking incubator, respectively. The overnight bacterial cultures were then diluted in fresh medium and an inoculum containing 2–5 $\times$ $10^6$ CFU/mL cells were transferred on top of graphene nanospikes of a growth time at 20 min. After 24 h incubating, biofilms on each substrate were detached by probe sonication, washed with 0.89 % NaCl solution, collected by centrifuge (5000 rmp, 5 min), and finally fixed by 10 mM N-ethylmaleimide (NEM) at room temperature for 2 h. To prepare a positive control, colonies harvested from the control surface (uncoated silicon substrate) were treated with 100 mM $H_2O_2$ for 40 min before fixation. Three as-prepared samples were then transferred to a microscope slide and observed under a Nikon ECLIPSE Ti2 inverted fluorescent microscope. The excitation wavelength ($\lambda_{ex}$) of oxidized channel and reduced channel was 405 nm and 488 nm, respectively. The emission wavelengths ($\lambda_{em}$) of both channels were set at 505–550 nm. Intensity ratio 405/488 nm was calculated from ten representative regions of interest using Image J software. For each sample, fluorescent images were taken for five random locations. Three independent biological replicates were assessed for each sample.

### 2.6. Biocompatibility of graphene nanospikes to mammalian cells

The cell viability of Huh7 human hepatoma cell line was evaluated by the standard alamarBlue assay, in order to assay the toxicity of graphene nanospikes toward mammalian cells. Huh7 cells were a kind gift from Prof. Elin K. Esbjörner, Division of Chemical Biology, Department of Life sciences, Chalmers University of Technology. The human cell line has been authenticated using STR (or SNP) profiling within the last three years. Cells were cultured in RPMI medium containing 10 % fetal bovine serum (FBS) in a humidified incubator of 5 % $CO_2$ at 37 °C. The graphene samples at a growth time of 20 min and silicon substrates were UV-sterilized before usage. Then, all samples were transferred to 24 well plates and seeded with Huh7 cells at a density of 0.8 $\times$ $10^5$ cells per well. After 24 h incubation, the old medium was discarded and fresh medium containing 1x alamarBlue (Thermo Scientific) was added separately to each well, following another 3 h incubation. The fluorescent signal of resorufin, which was a reduced product of resazurin by living cells, was detected using FLUOStar Omega microplate reader. The cell viability of different surfaces was normalized in reference to the medium control.

## 3. Results and discussion

### 3.1. Growth time controls key physical parameters of graphene nanospikes

To investigate the optimal nanofeatures of graphene for bacteria killing, we synthesized graphene nanospikes of different height, thickness, and edge/defect density by controlling growth time. Five samples coated with graphene nanospikes were assembled, and the coating morphologies were observed using SEM. As shown in Fig. 1a, graphene flakes of a leaf shape morphology appeared at a growth time of 10 min. The nanosheets became denser and taller with increasing growth time from 10 to 20 min. Another morphology, namely bloomed flower shape, emerged with longer growth times, at 25 and 30 min. With the emergence of bloomed flower shape, the total amount of sharp edges/defects was reduced drastically (at 25 and 30 min). Cross-sectional SEM was used to observe the orientation of graphene nanospikes. And it was shown that the graphene sheets of all five samples had partially vertical orientation relative to the substrate (Fig. S1). AFM was employed to further characterize the surface parameters of graphene nanostructures. By comparing three-dimensional AFM images of five graphene samples (Fig. S2), we observed a change of graphene morphology from sheet structure to cluster structure, accompanied by a decrease of edge/defect density. The turning point for this change was between 20 and 25 min, which was in line with the SEM results. The dimensions of the surface nanofeatures were analyzed carefully based on AFM height images with the scan area of 1 $\times$ 1 $\mu m^2$. The spatial distributions (spacing) of graphene arrays ranged from 30 to 400 nm. Longer growth times resulted in coatings with increased height and thickness (Fig. 2b and c) of graphene nanospikes. The average height of graphene nanospikes increased from 107 nm to 520 nm according to large area AFM scan results (Fig. S3 and

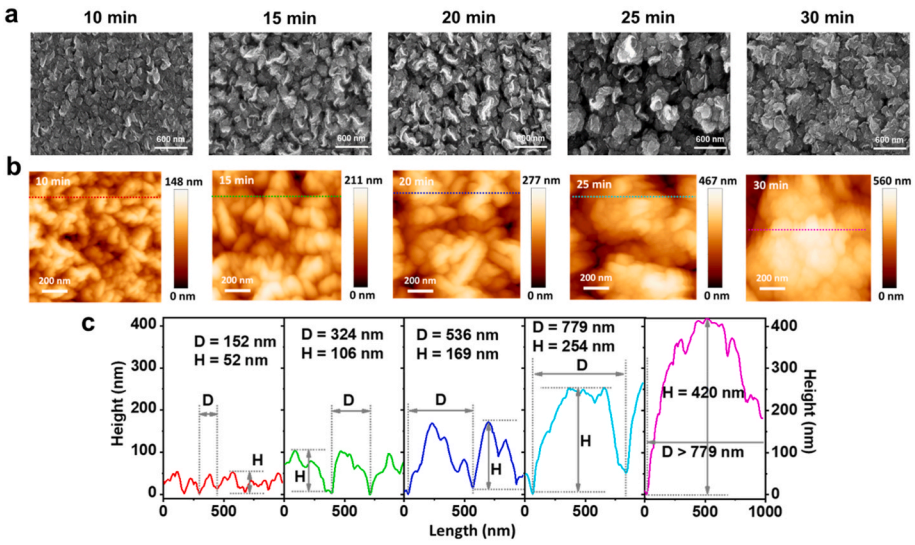


**Fig. 1.** Morphology and dimension characterization of graphene nanospikes. (a) SEM images of graphene nanospikes grown on silicon substrate at a growth time of 10, 15, 20, 25, and 30 min, respectively. (b) AFM height images of graphene nanospikes at different growth times. The scan area of AFM images was 1 × 1 μm$^2$. The dash lines in the images marked the positions where the cross-sectional profiles were extracted. (c) The correspondence cross-sectional profiles of each graphene sample extracted from AFM images above, showing the mean diameter (D) and the height (H) of graphene nanospikes produced at different growth times. (A colour version of this figure can be viewed online.)

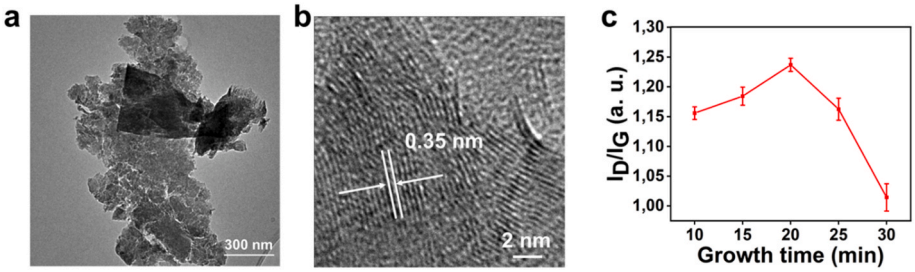


**Fig. 2.** Atomic structure characterization of graphene nanospikes. (a) TEM image of graphene nanospikes scratched from the substrate. (b) High-resolution TEM image of graphene nanospikes, demonstrating the atomic structure. (c) Quantification of defects density of graphene nanospikes at different growth time. The Raman intensity ratio of D peak and G peak ($I_D/I_G$) of graphene nanospikes was plotted as a function of growth time. (A colour version of this figure can be viewed online.)

**Table 1**
Surface parameters and antibacterial activity of graphene nanospikes.

| *Surface* | 10 min | 15 min | 20 min | 25 min | 30 min |
|---|---|---|---|---|---|
| *Surface characteristics* | | | | | |
| Height (nm) | 106.6 ± 9.9 | 130.3 ± 8.3 | 181.0 ± 6.6 | 303.3 ± 19.5 | 520.3 ± 6.5 |
| Ratio $I_D/I_G$ | 1.156 ± 0.011 | 1.184 ± 0.015 | 1.237 ± 0.011 | 1.162 ± 0.018 | 1014 ± 0.023 |
| Aspect ratio | 2.92 ± 0.13 | 3.06 ± 0.25 | 3.17 ± 0.19 | 3.07 ± 0.27 | 1.85 ± 0.30 |
| Water contact angle, θ (°) | 104.00 ± 0.08 | 114.21 ± 0.06 | 116.58 ± 0.12 | 134.69 ± 0.08 | 140.40 ± 0.30 |
| *Loss of viability (%)* | | | | | |
| *E. coli* | 12.6 ± 2.5 | 34.3 ± 2.6 | 61.1 ± 3.6 | 22.6 ± 4.0 | 10.7 ± 1.2 |
| *S. aureus* | 27.7 ± 3.2 | 53.2 ± 1.7 | 92.3 ± 3.8 | 43.1 ± 4.3 | 11.7 ± 1.5 |

Table 1 in supplementary information). The aspect ratio of graphene nanospikes at different growth times ranged from 1.85 to 3.17 (Table 1). However, we did not observe a lineally enhancement of aspect ratio when we prolonged the growth time of graphene. Instead, the highest aspect ratio was obtained on graphene sample at a growth time of 20 min. We propose that this change point of morphology and aspect ratio stems from two different growth stages of graphene, which has been reported by many researchers previously [36,37]. Generally, the growth mechanism of vertical graphene nanospikes includes three steps, which are nucleation, vertical growth, and saturation. In the first step, a horizontal buffer layer that contains mismatches and curved areas is formed on the substrate. Then, stemming from these nucleation sites, vertical graphene starts to grow continuously at the open edges/defects by carbon deposition, which explains why they become denser and higher from 10 to 20 min. Finally, vertical growth becomes saturated and new branches of flakes tend to grow out of the eroded areas of main spikes, due to plasma etching, which results in cluster structure with fewer exposed edges/defects.

The atomic structures of graphene nanospikes were confirmed using TEM. A representative TEM image (Fig. 2a) of nanospikes shows that graphene nanosheets were continuously growing on the substrate. High-resolution TEM identified high crystallinity of partially vertical graphene in certain areas (Fig. 2b). The lattice parameter was 0.35 nm, which is consistent with the spacing between two graphene nanosheet layers [37], suggesting that multi-layered graphene sheets were formed during growth. Raman spectrum (Fig. S4) displays three prominent peaks related to graphene [37], which are assigned as D-peak at around 1341 cm$^{-1}$, G-peak at approximately 1579 cm$^{-1}$, and 2D-peak at around 2868 cm$^{-1}$. Of particular interest for our study is the so-called defect/edge related D-peak. The intensity ratio of D- and G-band ($I_D/I_G$) determines the edge/defect density of graphene, whereby a higher ratio indicates less crystallinity and more defects [38]. As plotted from Raman

spectra, all five graphene samples had abundant edges/defects. The highest ratio $I_D/I_G$ was achieved at a growth time of 20 min (Fig. 2c), which was in agreement with our SEM and AFM observations. Altogether, we concluded the surface parameters of graphene nanostructures produced by PECVD on silicon substrate could be easily tailored by controlling growth time. Graphene nanospikes with the highest density of exposed edges/defects are achieved at a growth time of 20 min.

To evaluate the change of hydrophobicity of surface after coatings with graphene nanospikes, we characterized the surface wettability of each sample by measuring its water contact angle. Compared with hydrophilic silicon substrate which showed a water contact angle of 71 °C, surfaces that were coated with graphene nanostructures were converted to hydrophobic in all samples. The contact angles of substrates kept increasing when prolonging growth time from 10 to 30 min (Fig. S5 and Table 1 in supplementary information). Increasing hydrophobicity of a surface is known to repel microorganisms and reduce cell attachment, so from the perspective of antibiofilm activity, this is a beneficial property of graphene nanoarrays [11,39].

### 3.2. Bactericidal activity of graphene nanospikes depends on the density of edge/defect

To evaluate the influence of surface characteristics on toxicity, we tested antibacterial activity of all five coatings with graphene nanospikes on two types of pathogens: *E. coli* as a model organism for Gram-negative bacteria and *S. aureus* as a model of Gram-positive bacteria. Briefly, bacteria were cultured on different substrates for 24 h, after which biofilms were stained with a commercial kit which contained SYTO 9 and propidium iodide (PI). The green color of SYTO 9 indicates living cells, whereas red color of PI indicates dead cells (into which PI penetrates). As mentioned above, height and thickness of graphene nanospikes increased continuously with growth time, from 10 to 30 min. Density of defects/edges followed a different trend, initially increasing up until the emergence of the bloomed flower shape morphology (after 20 min) and continued decreasing thereafter. Live-dead staining results for both *S. aureus* and *E. coli* (Fig. 3) indicated that the extent of killing of bacteria correlated in a linear manner with density of defects/edges. Increase of height and thickness of the nanospikes correlated with the killing efficiency only initially, until the transition point of 20 min, when the morphology of the coating changed. So, the 20 min growth point, with maximal density of defects/edges, represents a clear optimum in terms of antibacterial effects of the graphene nanospikes coating.

To test these findings with an independent method, colony forming units (CFUs) counting of bacteria attached to the surface over periods up to 24 h was performed. The data were normalized to the CFU counts of bacteria adhered on bare silicon surfaces (without graphene nanospikes coating), taken as 100 % bacterial attachment. CFU counts on graphene-coated surfaces were fully consistent with live/dead staining results (Fig. 4). Specifically, graphene nanospikes at a growth time of 20 min exhibited the highest antibacterial activity at 92.3 % against *S. aureus* and at 61.1 % against *E. coli*, respectively (Fig. 4a). It has been proposed that physical parameters of the nanoarrays, for example height, thickness, and edge density, can influence the bactericidal efficiency [11], but the respective relevance of each of these features has not been

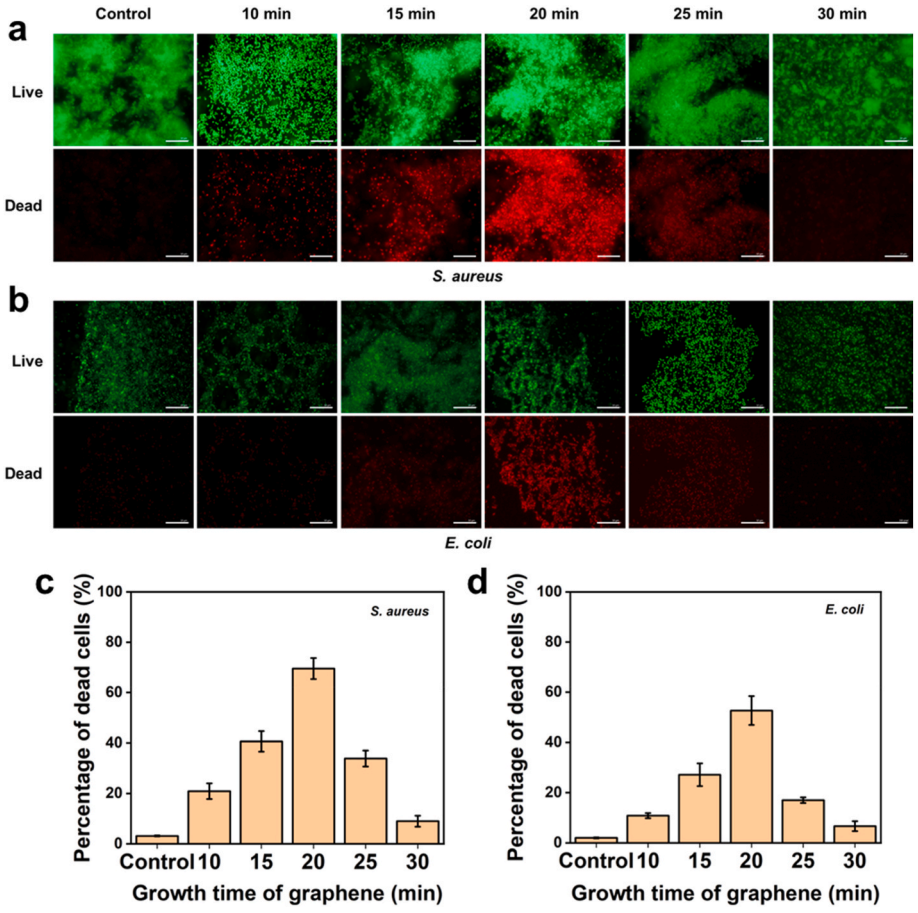


**Fig. 3.** Bactericidal activity of graphene nanospikes coated surfaces. (a, b) Live and dead stanning of *S. aureus* (a) and *E. coli* (b) after 24 h culture on graphene surfaces of different growth time. Silicone substrate coated with $SiO_2$ layer of 300 nm in thickness was treated as control. The colors are false colors, of which green represents live cells, while dead cells are shown in red color. Scale bar = 20 μm. (c, d) Quantification of nonviable *S. aureus* cells (c) and *E. coli* cells (d) attached on graphene coated surfaces. All experiments were performed in three biological replicates. (A colour version of this figure can be viewed online.)

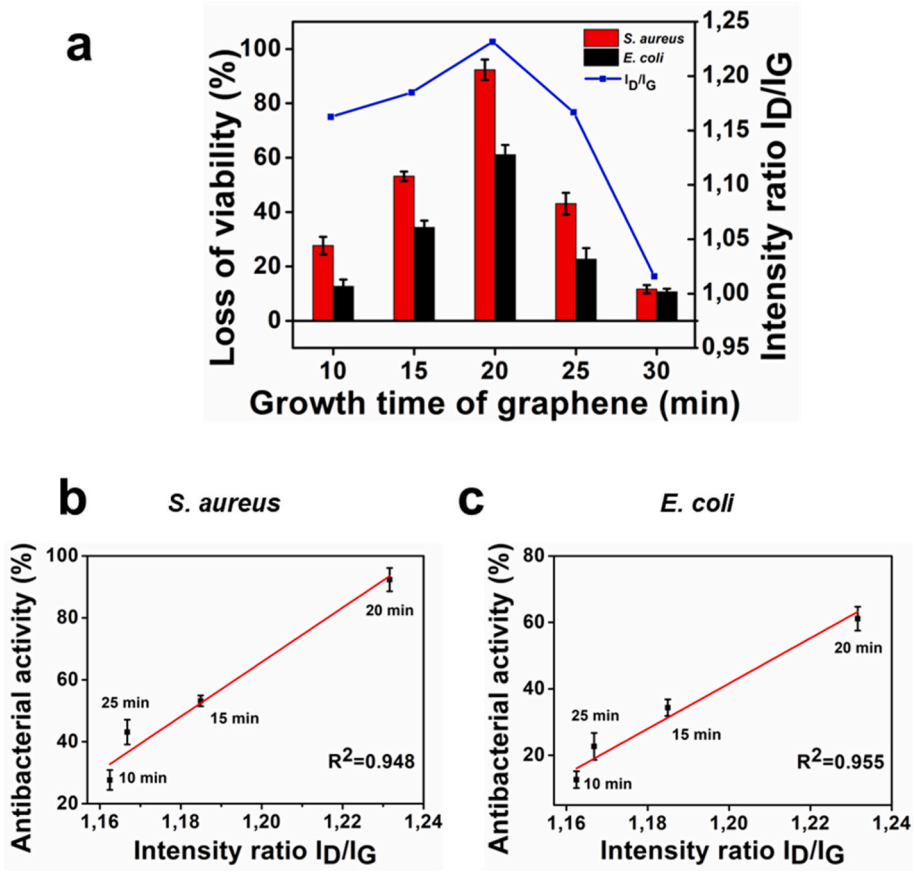


**Fig. 4.** Bactericidal activity of graphene nanospikes coated surfaces. (a) Cytotoxicity of graphene surfaces against *S. aureus* and *E. coli* corresponding to the growth time of graphene nanospikes (left axis), as well as the edge/defect density (Raman intensity ratio $I_D/I_G$) as a function of growth time of graphene (right axis). Both bacterial strains were cultured on graphene surfaces for 24 h. Surface-attached bacteria were then collected by mild sonication. Cell viability was obtained by CFU counting, normalized with data from non-coated silicon substrate. (b, c) Linear fitting of correction between antibacterial activity and the edge/defect density of graphene nanospikes. (A colour version of this figure can be viewed online.)

clearly understood. A recent report proposed that the density of exposed edges of graphene nanoplatelets in polymer composites represents the key determinant for antibacterial effects [40]. The authors argued that exposed edges preclude attachment of bacteria, and hence form bacteria-exclusion zones on the surface. From this assumption, they demonstrated that the predicted exclusion areas correlate perfectly with loss of bacterial attachment/viability. Along similar lines, our results suggest that the density of edges/defects is the main governing factor regarding antibacterial effects (Fig. 4). Increasing height and thickness of nanospikes, at the expense of density of edges/defects, proved to be counter-productive from the perspective of antibacterial effects.

Beside edge/defect-density-dependent bactericidal activity, our experimental data also suggested that the Gram-positive *S. aureus* is more sensitive to graphene nanospikes compared to Gram-negative bacteria *E. coli*. Differences in sensitivity between Gram-positive and Gram-negative bacteria have been debated previously. Some authors argued that the thickness of cell wall plays a dominant role in mitigating membrane stress upon contact with natural or biomimetic nanostructures [11,41]. In this regard, Gram-positive bacteria which possess thicker cell walls (ranging from 30 to 100 nm compared to 7–8 nm of Gram-negatives) are proposed to be less susceptible to rupture and deformation by nanostructures [5]. By contrast, Ivanova et al. reported that Gram-positive *S. aureus* was about 1.5-fold more sensitive to wing surface of dragonfly *Diplacodes bipunctata* compared to Gram-negative *Pseudomonas aeruginosa* [9]. In addition, it has been shown that *S. aureus* is more sensitive than *P. aeruginosa* to a graphene film with exposed sharp edges [24]. Moreover, graphene oxide nanowalls deposited on stainless steel also exhibited higher efficiency in inactivate *S. aureus* than *E. coli* [23]. One possible explanation is that the cell envelope of Gram-negative bacteria is more deformable than that of Gram-positives, requiring more force to compromise and break the membrane integrity [16,23,42]. The higher deformability of Gram-negatives may be in part conferred by the existence of the additional outer membrane (made of lipopolysaccharide), which is lacking in the Gram-positives such as *S. aureus* [23]. More theoretical and experimental studies will be required to settle this question.

All in all, our results suggest a straightforward criterion for optimizing antibacterial surfaces against both types of bacteria. By creating a maximum of exposed edges/defects during PECVD synthesis, one can fabricate graphene nanospikes with superior antibacterial properties.

### 3.3. Redox stress plays an important part in the antibacterial mechanism of graphene nanospikes

To assess the level of physical disruption caused by our surfaces, we examined the morphology of bacteria after a 24-h exposure to graphene nanospikes. Following the fixation and dehydration process, bacteria were observed under SEM. As expected, both bacterial species examined on the control surface of silicon substrates exhibited great density of cells and intact morphology. By contrast, much fewer cells were observed on surfaces coated with graphene nanospikes, demonstrating that the nanostructures effectively prevented biofilm from adhering to the surface (Fig. 5). Moreover, in the presence of graphene nanospikes, a significant deformation of cells was observable in most cells, resulting in either flattened or compressed cells, or ruptured cells. The results were similar for Gram-negative and -positive bacteria.

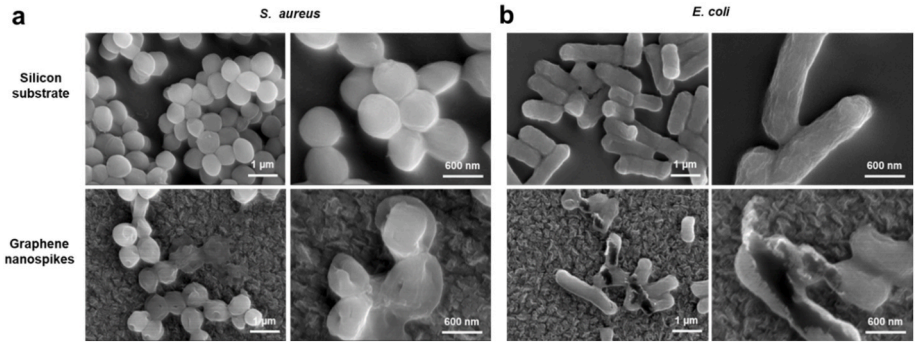


**Fig. 5.** Physical damage caused by graphene nanospikes. SEM images of *S. aureus* (a) and *E. coli* (b) after 24 h contact with graphene surfaces. Graphene surfaces grown for 20 min were chosen for this assay, since they possess the highest bactericidal activity. (A colour version of this figure can be viewed online.)

Some of the previous studies have suggested that physical disruption is the main factor in the antibacterial mechanism of vertically aligned graphene nanospikes, and that these surfaces are less likely to induce ROS production or oxidative stress in bacteria [28]. Other studies claimed that oxidative stress may also be responsible for the toxicity of graphene surfaces due to direct electron transfer from cell membrane to the surface without producing ROS [25,29]. Herein, we attempted to settle this debate on whether oxidative damage plays a role for the bactericidal effect of graphene nanospikes aligned on a surface. For this purpose, a commercial fluorescent ROS probe, CellROX™ Deep Red Reagent, was first employed to stain bacteria that were grown on substrates for 24 h. Bacteria grown on silicon substrate without graphene coating were used as a negative control, and biofilms exposed to 100 mM $H_2O_2$ for 40 min before staining with CellRox were used as a positive control for ROS stress. According to the CellRox manufacturer, this fluorescent dye is reactive to most of the chemical species included in ROS, including hydroxyl radical (•OH), superoxide radical anion ($O_2$•−), hydrogen peroxide ($H_2O_2$), peroxynitrite ($ONOO^-$), nitric oxide (•NO) and *tert*-butyl hydroperoxide (TBHP). The fluorescent emission of oxidized probe at 655 nm was recorded by fluorescent microscope. As shown in Figs. S6 and S7, hydrogen peroxide treated cells exhibited strong fluorescent signal in the CellRox channel. And a relatively slight increase of ROS level was detected in both *S. aureus* and *E. coli* strains after graphene nanospikes treatment, compared with control group. However, owing to the intrinsic limitations of this small-molecule probe (discussed before) and owing to the short lifespan of most ROS species, we could not obtain fluorescent images with sufficient resolution and quality. The challenge of monitoring dynamic redox state in living cells requires more powerful and precise tools.

Genetically encoded redox biosensors have provided major advances in real-time measuring of oxidative damage in living cells, in terms of quick response, unprecedented sensitivity, and temporal resolution [32–34]. Generally, redox biosensors can specifically catalyze the equilibration between one redox pair in cells, accompanied by a ratiometrical change of the excitation wavelength of such probes. This is a god proxy for representing the overall redox state of cells and indicating oxidative stress. Taking advantage of those biosensors, we aimed to detect and quantify oxidative stress in bacteria triggered by graphene nanospikes. Specifically, we used a commercially available protein probe called Grx1-roGFP2 (created by Dick et al.) to measure the glutathione (GSH)/glutathione disulfide (GSSG) redox couple in *E. coli* cells [33]. To avoid impairing the redox status of the biosensor by additional handling, cells were detached from the tested surfaces and treated with 10 μM N-ethyl maleimide (NEM) before taking images using fluorescent microscope, as described in the literature [35]. The fluorescent emission intensity of the sensor at 505–550 nm was recorded by excitation at 405 nm and 488 nm. The oxidized channel (405 nm channel) and the reduced channel (488 nm channel) are false-colored in red and green, respectively. Addition of $H_2O_2$ as a positive control for ROS stress resulted in a drastic increase of fluorescent intensity in the 405 nm-excited channel, demonstrating that cells underwent considerable oxidative damage. According to the previous study, the damage was irreversible [34], which makes our positive control stable and reproducible. Graphene nanospikes also caused a strong oxidative signal in *E. coli* cells, compared to that of silicon surface (Fig. 6). The degree of oxidation (OxD) was quantified by calculating the fluorescent intensity ratio 405/488 nm, whereby higher percentage means more oxidative damage. As shown in Fig. 6b, the level of oxidation in *E. coli* cells incubated on graphene nanospikes surface had a 2.9-fold increase compared to the negative control, whereby OxD in the positive control underwent a 5.3-fold increase. A standard Student's *t*-test showed that there was a statistically significant difference between oxidative state of *E. coli* cells grown on coated and noncoated surfaces.

Following the same principle, we also monitored the bacillithiol (BSH) redox potential in *S. aureus* using a biosensor named Brx-rpGFP2, developed by Antelmann and coworkers [34]. Since most Gram-positive bacteria employ BSH as a dominant antioxidant instead of GSH, the dynamic change of BSH could inform the oxidative state of *S. aureus* cells [43]. The results demonstrated that graphene surface also increased the oxidation level of *S. aureus* cells by approximately 2.6-fold (Fig. S8). From these quantitative data, we could confidently conclude that bacteria underwent notable oxidative stress upon contact with graphene nanospikes, regardless of bacterial species. Altogether, our results indicate that the graphene nanospikes are not only able to prevent bacteria attachment, but also kill bacteria that adhered on the surface through the synergistic effect of mechanical disruption and oxidative damage (Fig. 7). Those excellent properties make graphene nanostructures very suitable for developing antibacterial coatings.

### 3.4. Graphene nanospikes are safe for human cell lines

Finally, we assessed the biocompatibility of graphene nanospikes on the Huh7 human hepatoma cell line. A standard alamarBlue assay was used to quantify cell viability upon a 24 h period of exposure to graphene nanospikes. Cells grown on a silicon surface were used as a control. As shown in Fig. 8, the graphene coating with the highest antibacterial efficiency (growth time of 20 min) was harmless to Huh 7 cells, with no significant decrease of cell viability. This result is in agreement with previous reports that mammalian cells experienced no significant membrane stress upon contact with natural or chemically synthesized surfaces with nanoarrays [11,44,45].

## 4. Conclusions

Our work demonstrates that nanostructured graphene exerts bactericidal effect possibly through adhesion prevention and contact killing of bacterial cells. The method we exploit for fabricating graphene nanospikes on the substrate, namely PECVD, is a single-step process and

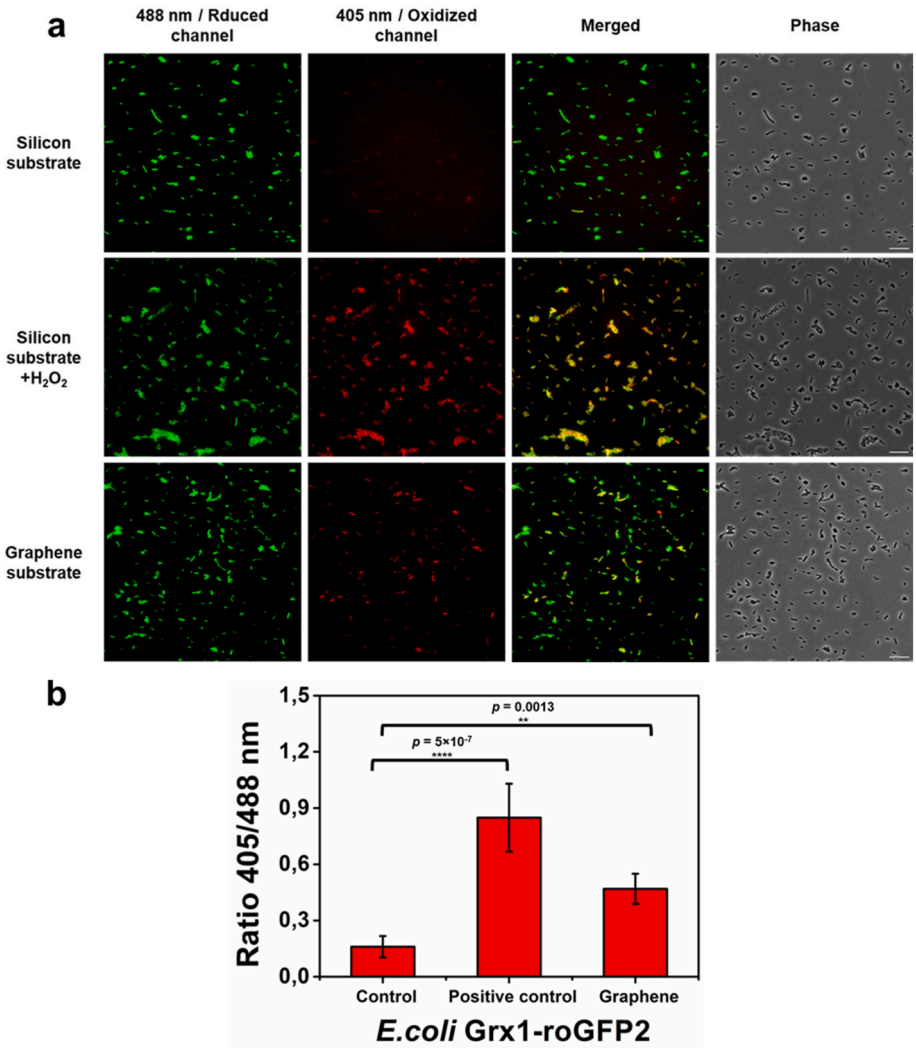


**Fig. 6.** Oxidative stress caused by graphene nanospikes. (a) Live imaging of *E. coli* Grx1-roGFP2 cells cultured on silicon substrate and graphene-coated surface after 24 h. To set a stable positive control for oxidative stress, 24 h-old biofilm detached from silicon substrate was exposed to 100 mM $H_2O_2$ for 40 min. Cells were gently detached from the surfaces, washed with PBS buffer for three times, blocked with 10 μM NEM for 2 h in room temperature, and analyzed using fluorescent microscopy. The excitation wavelength was 405 and 488 nm, respectively. And the fluorescence images were collected the signals from 505 to 550 nm for both channels. The biosensor in oxidized state and in reduced state was false-colored in red and green, respectively. Scale bar = 5 μm (b) The average intensity ratio 405/488 nm of three *E. coli* samples were calculated from ten representative regions of interest in the corresponding fluorescent images. *p*-values were calculated using a Student's two-tailed *t*-test. Symbols are defined as follows: $^{**}p \leq 0.01$; $^{****}p \leq 0.0001$. (A colour version of this figure can be viewed online.)

allows for fine tuning of nanofeatures in a highly reproducible manner. One important outcome of our study is that we have identified the density of edges/defects as the key parameter for effectiveness of antibacterial coatings. Consequently, we demonstrate that other parameters, such as height and thickness nanospikes, do not directly correlate with bactericidal effects. This may offer a valuable guideline for further improving the bactericidal efficiency of coatings based on GMs. Furthermore, using genetically encoded biosensors, we provide evidence that oxidative damage contributes to antibacterial effects of graphene coatings. Combining the ability of mechanically rupturing bacterial membranes with significant redox stress, our graphene coatings represent a promising biomimetic nanostructure capable of mitigating surface contamination caused by bacteria.

## Notes

The authors declare no competing financial interest.

## Funding

This work was founded by VINNOVA to I. M. and Vetenskapsrådet to S·P.

## CRediT authorship contribution statement

**Yanyan Chen:** Conceptualization, Methodology, Validation, Investigation, Writing – original draft, Writing – review & editing, and, Visualization. **Santosh Pandit:** Conceptualization, Methodology, Writing – original draft, Writing – review & editing, Supervision, Project administration, and, Funding acquisition. **Shadi Rahimi:** Methodology, Investigation, and, Writing – original draft. **Ivan Mijakovic:** Conceptualization, Writing – original draft, Writing – review & editing, Supervision, and, Funding acquisition.

## Declaration of competing interest

The authors declare that they have no known competing financial interests or personal relationships that could have appeared to influence

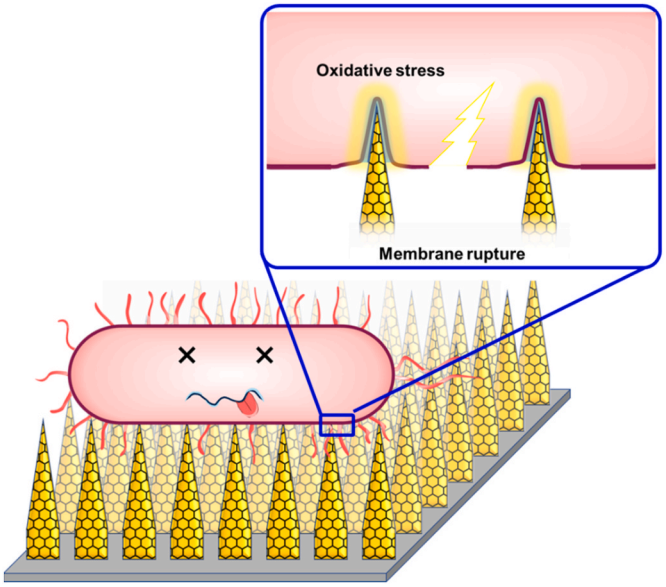


**Fig. 7.** Schematic illustration of the synergistic antibacterial mechanism of graphene nanospikes. (A colour version of this figure can be viewed online.)

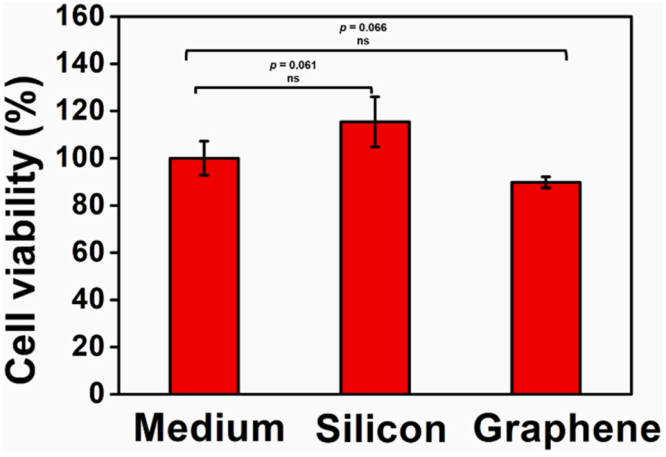


**Fig. 8.** Biocompatibility of graphene nanospikes. Cell viability of Huh-7 cells after 24 h of contact with silicon substrate coated with graphene nanospikes at a growth time of 20 min. *p*-values are calculated using a Student's two-tailed *t*-test. Symbol is defined as follows: $^{ns}p > 0.05$. (A colour version of this figure can be viewed online.)

the work reported in this paper.

## Acknowledgements

We acknowledge the funding provided by 2D TECH VINNOVA competence Center (Ref. 2019–00068). We acknowledge instrumental support from Chalmers Materials Analysis Laboratory (CMAL) and MC2 Chalmers Nanofabrication Laboratory. The authors are grateful to Tobias Dick for providing the plasmid pQE-60 Grx1-roGFP2-His and to Mikael Molin from Chalmers University of Technology for the expression of GSH biosensor in *E. coli* strain. The *S. aureus* COL stains containing pRB437-XylR-Brx-roGFP2 plasmid is a kind gift from Vu Van Loi and Haike Antelmann of Freie University. The authors would also like to thank Ann-Britt Schäfer and Michaela Wenzel from Chalmers University of Technology for the help with live imaging of oxidative stress using fluorescent microscopy.

## Appendix A. Supplementary data

Supplementary data to this article can be found online at https://doi.org/10.1016/j.carbon.2023.118740.

## References

[1] K.S. Ikuta, L.R. Swetschinski, G. Robles Aguilar, F. Sharara, T. Mestrovic, A.P. Gray, et al., Global mortality associated with 33 bacterial pathogens in 2019: a systematic analysis for the Global Burden of Disease Study 2019, Lancet 400 (10369) (2022) 2221–2248.
[2] X. Ding, S. Duan, X. Ding, R. Liu, F.-J. Xu, Versatile antibacterial materials: an emerging arsenal for combatting bacterial pathogens, Adv. Funct. Mater. 28 (40) (2018), 1802140.
[3] Y. Wang, Y. Yang, Y. Shi, H. Song, C. Yu, Antibiotic-free antibacterial strategies enabled by nanomaterials: progress and perspectives, Adv. Mater. 32 (18) (2020), 1904106.
[4] N. Lin, P. Berton, C. Moraes, R.D. Rogers, N. Tufenkji, Nanodarts, nanoblades, and nanospikes: mechano-bactericidal nanostructures and where to find them, Adv. Colloid Interface Sci. 252 (2018) 55–68.
[5] A. Tripathy, P. Sen, B. Su, W.H. Briscoe, Natural and bioinspired nanostructured bactericidal surfaces, Adv. Colloid Interface Sci. 248 (2017) 85–104.
[6] E.P. Ivanova, J. Hasan, H.K. Webb, V.K. Truong, G.S. Watson, J.A. Watson, et al., Natural bactericidal surfaces: mechanical rupture of Pseudomonas aeruginosa cells by cicada wings, Small 8 (16) (2012) 2489–2494.
[7] S.M. Kelleher, O. Habimana, J. Lawler, B. O' Reilly, S. Daniels, E. Casey, et al., Cicada wing surface topography: an investigation into the bactericidal properties of nanostructural features, ACS Appl. Mater. Interfaces 8 (24) (2016) 14966–14974.
[8] D.E. Mainwaring, S.H. Nguyen, H. Webb, T. Jakubov, M. Tobin, R.N. Lamb, et al., The nature of inherent bactericidal activity: insights from the nanotopology of three species of dragonfly, Nanoscale 8 (12) (2016) 6527–6534.
[9] E.P. Ivanova, J. Hasan, H.K. Webb, G. Gervinskas, S. Juodkazis, V.K. Truong, et al., Bactericidal activity of black silicon, Nat. Commun. 4 (1) (2013) 2838.
[10] J. Jenkins, J. Mantell, C. Neal, A. Gholinia, P. Verkade, A.H. Nobbs, et al., Antibacterial effects of nanopillar surfaces are mediated by cell impedance, penetration and induction of oxidative stress, Nat. Commun. 11 (1) (2020) 1626.
[11] B. Mehrjou, Y. Wu, P. Liu, G. Wang, P.K. Chu, Design and properties of antimicrobial biomaterials surfaces, Adv. Healthcare Mater. 12 (16) (2022), 2202073.
[12] S. Park, H.-H. Park, K. Sun, Y. Gwon, M. Seong, S. Kim, et al., Hydrogel nanospike patch as a flexible anti-pathogenic scaffold for regulating stem cell behavior, ACS Nano 13 (10) (2019) 11181–11193.
[13] G. Wang, W. Jiang, S. Mo, L. Xie, Q. Liao, L. Hu, et al., Nonleaching antibacterial concept demonstrated by in situ construction of 2D nanoflakes on magnesium, Adv. Sci. 7 (1) (2020), 1902089.
[14] M. Michalska, F. Gambacorta, R. Divan, I.S. Aranson, A. Sokolov, P. Noirot, et al., Tuning antimicrobial properties of biomimetic nanopatterned surfaces, Nanoscale 10 (14) (2018) 6639–6650.
[15] D.P. Linklater, M. De Volder, V.A. Baulin, M. Werner, S. Jessl, M. Golozar, et al., High aspect ratio nanostructures kill bacteria via storage and release of mechanical energy, ACS Nano 12 (7) (2018) 6657–6667.
[16] S.L. Arias, J. Devorkin, J.C. Spear, A. Civantos, J.P. Allain, Bacterial envelope damage inflicted by bioinspired nanostructures grown in a hydrogel, ACS Appl. Bio Mater. 3 (11) (2020) 7974–7988.
[17] D.P. Linklater, H.K.D. Nguyen, C.M. Bhadra, S. Juodkazis, E.P. Ivanova, Influence of nanoscale topology on bactericidal efficiency of black silicon surfaces, Nanotechnology 28 (24) (2017), 245301.
[18] C. Cheng, S. Li, A. Thomas, N.A. Kotov, R. Haag, Functional graphene nanomaterials based architectures: biointeractions, fabrications, and emerging biological applications, Chem. Rev. 117 (3) (2017) 1826–1914.
[19] H. Ji, H. Sun, X. Qu, Antibacterial applications of graphene-based nanomaterials: recent achievements and challenges, Adv. Drug Deliv. Rev. 105 (2016) 176–189.
[20] X. Zou, L. Zhang, Z. Wang, Y. Luo, Mechanisms of the antimicrobial activities of graphene materials, J. Am. Chem. Soc. 138 (7) (2016) 2064–2077.
[21] Y. Chen, S. Pandit, S. Rahimi, I. Mijakovic, Interactions between graphene-based materials and biological surfaces: a review of underlying molecular mechanisms, Adv. Mater. Interfac. 8 (24) (2021), 2101132.
[22] W. Han, Z. Wu, Y. Li, Y. Wang, Graphene family nanomaterials (GFNs)—promising materials for antimicrobial coating and film: a review, Chem. Eng. J. 358 (2019) 1022–1037.
[23] O. Akhavan, E. Ghaderi, Toxicity of graphene and graphene oxide nanowalls against bacteria, ACS Nano 4 (10) (2010) 5731–5736.
[24] V.T.H. Pham, V.K. Truong, M.D.J. Quinn, S.M. Notley, Y. Guo, V.A. Baulin, et al., Graphene induces formation of pores that kill spherical and rod-shaped bacteria, ACS Nano 9 (8) (2015) 8458–8467.
[25] X. Lu, X. Feng, J.R. Werber, C. Chu, I. Zucker, J.-H. Kim, et al., Enhanced antibacterial activity through the controlled alignment of graphene oxide nanosheets, Proc. Natl. Acad. Sci. USA 114 (46) (2017) E9793.
[26] N.-C. Yeh, C.-C. Hsu, J. Bagley, W.-S. Tseng, Single-step growth of graphene and graphene-based nanostructures by plasma-enhanced chemical vapor deposition, Nanotechnology 30 (16) (2019), 162001.
[27] W. Zheng, X. Zhao, W. Fu, Review of vertical graphene and its applications, ACS Appl. Mater. Interfaces 13 (8) (2021) 9561–9579.

[28] S. Pandit, Z. Cao, V.R.S.S. Mokkapati, E. Celauro, A. Yurgens, M. Lovmar, et al., Vertically aligned graphene coating is bactericidal and prevents the formation of bacterial biofilms, Adv. Mater. Interfac. 5 (7) (2018), 1701331.
[29] W. Wei, J. Li, Z. Liu, Y. Deng, D. Chen, P. Gu, et al., Distinct antibacterial activity of a vertically aligned graphene coating against Gram-positive and Gram-negative bacteria, J. Mater. Chem. B 8 (28) (2020) 6069–6079.
[30] X. Zhang, J. Qiu, J. Tan, D. Zhang, L. Wu, Y. Qiao, et al., In-situ growth of vertical graphene on titanium by PECVD for rapid sterilization under near-infrared light, Carbon 192 (2022) 209–218.
[31] P. Zhang, Z. Guo, C. Chen, I. Lynch, Uncertainties in the antibacterial mechanisms of graphene family materials, Nano Today 43 (2022), 101436.
[32] M.P. Murphy, H. Bayir, V. Belousov, C.J. Chang, K.J.A. Davies, M.J. Davies, et al., Guidelines for measuring reactive oxygen species and oxidative damage in cells and in vivo, Nat. Metab. 4 (6) (2022) 651–662.
[33] M. Gutscher, A.-L. Pauleau, L. Marty, T. Brach, G.H. Wabnitz, Y. Samstag, et al., Real-time imaging of the intracellular glutathione redox potential, Nat. Methods 5 (6) (2008) 553–559.
[34] V.V. Loi, M. Harms, M. Müller, N.T.T. Huyen, C.J. Hamilton, F. Hochgräfe, et al., Real-time imaging of the bacillithiol redox potential in the human pathogen Staphylococcus aureus using a genetically encoded bacilliredoxin-fused redox biosensor, Antioxid. Redox Signaling 26 (15) (2017) 835–848.
[35] V. Van Loi, H. Antelmann, Method for measurement of bacillithiol redox potential changes using the Brx-roGFP2 redox biosensor in Staphylococcus aureus, MethodsX 7 (2020), 100900.
[36] J. Zhao, M. Shaygan, J. Eckert, M. Meyyappan, M.H. Rümmeli, A growth mechanism for free-standing vertical graphene, Nano Lett. 14 (6) (2014) 3064–3071.
[37] Z. Bo, Y. Yang, J. Chen, K. Yu, J. Yan, K. Cen, Plasma-enhanced chemical vapor deposition synthesis of vertically oriented graphene nanosheets, Nanoscale 5 (12) (2013) 5180–5204.
[38] R. Sharma, J.H. Baik, C.J. Perera, M.S. Strano, Anomalously large reactivity of single graphene layers and edges toward electron transfer chemistries, Nano Lett. 10 (2) (2010) 398–405.
[39] S. Pandit, K. Gaska, V.R.S.S. Mokkapati, E. Celauro, A. Derouiche, S. Forsberg, et al., Precontrolled alignment of graphite nanoplatelets in polymeric composites prevents bacterial attachment, Small 16 (5) (2020), 1904756.
[40] S. Rahimi, T. Lovmar, A. Aulova, S. Pandit, M. Lovmar, S. Forsberg, et al., Automated prediction of bacterial exclusion areas on SEM images of graphene–polymer composites, Nanomaterials 13 (10) (2023) 1605.
[41] J. Hasan, H.K. Webb, V.K. Truong, S. Pogodin, V.A. Baulin, G.S. Watson, et al., Selective bactericidal activity of nanopatterned superhydrophobic cicada Psaltoda claripennis wing surfaces, Appl. Microbiol. Biotechnol. 97 (20) (2013) 9257–9262.
[42] P. Eaton, J.C. Fernandes, E. Pereira, M.E. Pintado, F. Xavier Malcata, Atomic force microscopy study of the antibacterial effects of chitosans on Escherichia coli and Staphylococcus aureus, Ultramicroscopy 108 (10) (2008) 1128–1134.
[43] G.L. Newton, M. Rawat, J.J. La Clair, V.K. Jothivasan, T. Budiarto, C.J. Hamilton, et al., Bacillithiol is an antioxidant thiol produced in Bacilli, Nat. Chem. Biol. 5 (9) (2009) 625–627.
[44] C. Mas-Moruno, B. Su, M.J. Dalby, Multifunctional coatings and nanotopographies: toward cell instructive and antibacterial implants, Adv. Healthcare Mater. 8 (1) (2019), 1801103.
[45] L. Hanson, Z.C. Lin, C. Xie, Y. Cui, B. Cui, Characterization of the cell–nanopillar interface by transmission electron microscopy, Nano Lett. 12 (11) (2012) 5815–5820.